Cement and Concrete Research 42 (2012) 265–271

Contents lists available at SciVerse ScienceDirect

Cement and Concrete Research

journal homepage: http://ees.elsevier.com/CEMCON/default.asp

Fire spalling of concrete, as studied by NMR

G.H.A. van der Heijden [a], L. Pel [a,*], O.C.G. Adan [a,b]

[a] Department of Applied Physics, Transport in Permeable media, Eindhoven University of Technology, P.O. Box 513, 5600 MB Eindhoven, The Netherlands
[b] TNO, Delft, The Netherlands

ARTICLE INFO

Article history:
Received 17 June 2011
Accepted 28 September 2011

Keywords:
Thermal analysis (B)
Degradation (C)
Permeability (C)
Transport properties (C)
Concrete (E)

ABSTRACT

The moisture transport in concrete subjected to fire is one of the most important processes with respect to fire spalling. The research on fire spalling of concrete is currently lacking experimental information of the moisture transport processes.

We present combined moisture content and temperature profiles of one-sided heated concrete samples measured with our dedicated NMR setup. The concrete samples were equilibrated at different moisture contents ranging from 97 to 50% RH. The moisture content can be measured quantitatively and non-destructively while heating up the sample one-sided to 500 °C.

We present the first experimental proof for the build up of a moisture peak in concrete, and the formation of a saturated layer. The temperatures measured at the boiling front indicate a vapour pressure in the order of 1.8 MPa. A simple vapour transport model was successfully used to describe the speed of the boiling front.

1. Introduction

The moisture content and transport in concrete, together with the vapour permeability, is presumed to be one of the most influential factors for fire spalling. It is generally assumed that below a certain moisture content of approximately 5 vol.% no spalling will occur [1,2]. Numerous heat and mass transfer models have been used to predict the moisture transport and its consequences on the strength and permeability of the concrete [3–11]. However, these models are only of use if they can be validated. For model validation, quantitative measurements of the evolution of moisture, temperature, and possibly pressure distributions in time are needed.

A few (indirect) observations of the moisture content in concrete have been reported in literature. Water has been observed bleeding from the cool side of a concrete wall, indicating that the surface layer is saturated [12]. Jansson et al. report a method in which a concrete cube is heated from one side. By splitting the heated cube in half, a layer with a relative higher saturation is observed by a discolouration of the concrete [13]. In this way, the sample is destroyed by the act of measurement itself. It will be extremely labourious to obtain a time evolution of the moisture content. Each time increment would also be from a different concrete sample. Experimentally determined moisture contents with a spatial resolution of about 20 cm were presented in a paper by Ichikawa et al. [14]. However, the obtained resolution is far too low to validate the model results.

With a dedicated NMR fire spalling setup it is possible to measure both the moisture and temperature distributions non destructively. This setup has been extensively tested in previous experiments on benchmark materials such as fired-clay brick, calcium silicate brick, and gypsum [16,17]. For the measurements on concrete it is necessary to have a validated measurement technique since the moisture content of concrete in equilibrium with, e.g., 50% RH, is typically in the range of 10^{-3} m^3 m^{-3}. Although the low moisture content is challenging the capabilities of the NMR setup, it was possible to measure the moisture transport in concrete.

In this paper we will present for the first time the combined moisture and temperature profiles in concrete. By combining these two parameters it is possible to estimate the vapour pressure inside the concrete samples. The paper is organised as follows. In Section 2 the materials and methods are presented. The results from the one-sided heating experiments are presented in Section 3. A discussion of the obtained results and final conclusions will be given in Section 4.

2. Material and methods

2.1. NMR setup

The fire spalling experiments were performed using a home-built NMR setup, which was especially designed for non-isothermal moisture measurements on building materials. A schematic diagram of this setup is shown in Fig. 1. The setup can be placed entirely in the bore of a 1.5 T whole-body medical scanner (Gyroscan, Philips), which is used only for its main magnetic field. Two coils, in an anti-Helmholtz configuration, with a diameter of 35 cm, provide a constant magnetic field gradient

* Corresponding author. Tel.: +31 402473406; fax: +31 402432598.
E-mail address: l.pel@tue.nl (L. Pel).

0008-8846/$ – see front matter © 2011 Elsevier Ltd. All rights reserved.
doi:10.1016/j.cemconres.2011.09.014

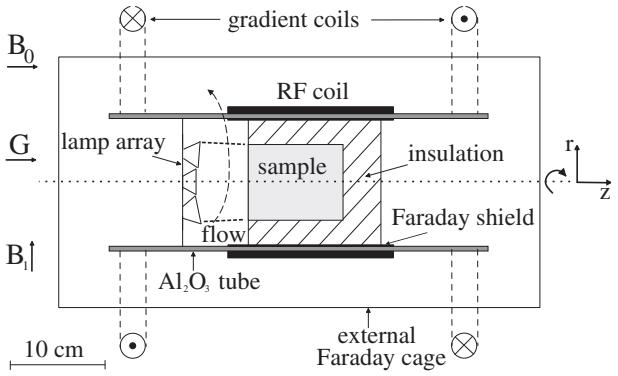

Fig. 1. Schematic diagram of the NMR setup. The setup has a cylindrical symmetry. A whole-body 1.5 T MRI scanner provides the main magnetic field B_0. Two coils in an anti-Helmholtz configuration provide a constant magnetic field gradient G. A bird-cage RF coil with a diameter of 140 mm is used for both sending the RF pulses B_1 and receiving the NMR signal. The bird-cage coil is constructed on an aluminium oxide (Al_2O_3) tube. An array of four 100 W halogen lamps is used to heat the sample, which is thermally insulated and positioned in the bird-cage coil.

G in the direction of B_0. In the experiments the gradient is set to 100 mT m^{-1}, providing a spatial resolution in the order of 3–5 mm.

A home built birdcage coil is used for sending the RF pulses (B_1) and receiving the NMR signal from the sample. The coil is 140 mm long and has a diameter of 140 mm. It is constructed using copper strips which are wrapped around an Al_2O_3 tube. A birdcage type coil is used because it generates a homogeneous B_1 field perpendicular to the long axis of the cylindrical sample. Therefore, the coil can be placed parallel to the main magnetic field, providing optimal use of the available space inside the bore. The coil is designed with an internal Faraday shield, in order to prevent changes in the dielectric constant of the drying sample from de-tuning the RF coil [18]. In this way, quantitative moisture content profiles can be obtained.

The Al_2O_3 tube can withstand temperatures far above the requirements of the experiments (melting temperature 2072 °C). Furthermore, it does not give any background signal, which is important when measuring a moisture content as low as 10^{-3} m^3 m^{-3} in concrete at high temperatures. In order to simulate the conditions as they occur in a fire, the concrete has to be heated up quickly. With an array of four 100 W halogen lamps, capable of generating a heat flux of 12 kW m^{-2}, we are able to mimic a 'fire' inside the NMR setup. The reflectors of the lamps are gold plated to ensure maximum reflection of infrared radiation towards the sample surface. Gold is used because it has a very high infra-red reflectivity of 0.98 and it does not oxidise [19]. To minimise heating of the RF coil, the lamp array is actively cooled. The heat flux from the lamp was calibrated calorimetrically and varies linearly with the applied electrical power to the lamp [16]. The maximum temperature which can be reached at the heated surface is about 400 to 500 °C. Although we do not reach the maximum temperatures occurring in a real life fire (~1000 °C), we are in the region of temperatures where the most interesting moisture related processes occur, such as boiling at temperatures higher than 100 °C, moisture clogging, and dehydration of the concrete. The temperatures are measured with type-K thermocouples, which were fitted in pre-drilled holes approximately 1 mm wide and 5 mm deep.

2.2. Concrete samples

The cylindrical concrete samples were drilled from larger cast blocks of $40\times10\times10$ cm^3 and have a diameter of 80 mm, and a length of 100 mm. The concrete has a strength class of C40, with a water cement ratio of 0.5. The details of the mix are given in Table 1. As can be seen, the largest aggregate size has been reduced to 8 mm to ensure a more representative sample volume. The concrete blocks were stored under water for 3 months before the samples were drilled. After drilling, four samples were first dried, after which they were equilibrated at four different relative humidities of 50%, 75%, 86%, and 97% RH until a constant mass was reached. The samples were 1 year old at the time of the experiment.

Table 1
Concrete mix design.

Constituent	Amount [kg m^{-3}]
CEM I 32.5 R	350
Water	175
Sand (0.125–0.250)	127
Sand (0.250–0.500)	217
Sand (0.500–1)	217
Sand (1–2)	253
Sand (2–4)	380
Grave (4–8 mm)	614
Total	2330

The concrete was characterised with mercury intrusion porosimetry (MIP), moisture sorption, and NMR. The MIP curve and the sorption isotherm of the concrete are shown in Fig. 2. From the MIP curve we can conclude that the dominant pore size is between 10 and 100 nm. The sorption isotherm curve shows an increase in moisture content already at a very low RH, which is in agreement with a dominant pore size in the nanometer range. Before the experiment, the samples were pressed in a PTFE holder to seal all sides except for the heated surface (transversal plane of the cylinder). In this way the moisture transport is limited to one dimension. The flow of heat is limited to one dimension by insulating the sample using mineral wool (4 cm). Numerical simulations indicate that the radial heat flow is limited to 10% of the longitudinal heat flow.

At the start of the experiment one moisture and temperature profile is measured to record the initial state of the sample. The first moisture profile is used to normalise subsequent profiles. In this way the moisture profiles are also corrected for the longitudinal inhomogeneity of the RF field. After the first profile is measured the heating is started. A constant heat flux of 12 kW m^{-2} is applied. To prevent hot vapour from condensing on cold surfaces inside the coil, air of 1–2% RH was blown over the sample surface. The air flow also ensures a constant boundary condition for the sample surface. The moisture and temperature profiles are measured every 7–10 min, depending on the number of averages needed.

The signal profiles measured with NMR have to be corrected for the temperature at which they were measured. Both the magnitude (magnetisation) and the time dependence (relaxation) of the NMR signal are temperature dependent. The correction procedure to obtain a quantitative moisture content was introduced and demonstrated in [15].

2.3. NMR calibration

In order to obtain a quantitative moisture content, the NMR signal must be calibrated against the moisture content of the concrete. For this purpose, the NMR signal was measured with the same settings as during the experiments. A sample was initially vacuum saturated, after which it was dried slowly to keep the moisture homogeneously distributed throughout the sample. Mass and signal were both recorded throughout the drying process. The NMR signal is shown as a function of the normalised sample mass in Fig. 3. For mass ratios between 1 and 0.94 a linear relation between the NMR signal and the moisture content is obtained. This indicates that the NMR signal can be directly related to the amount of free moisture present in the concrete.

After the sample was dried at ambient temperatures a further decrease in moisture content (adsorbed and chemically bound moisture)

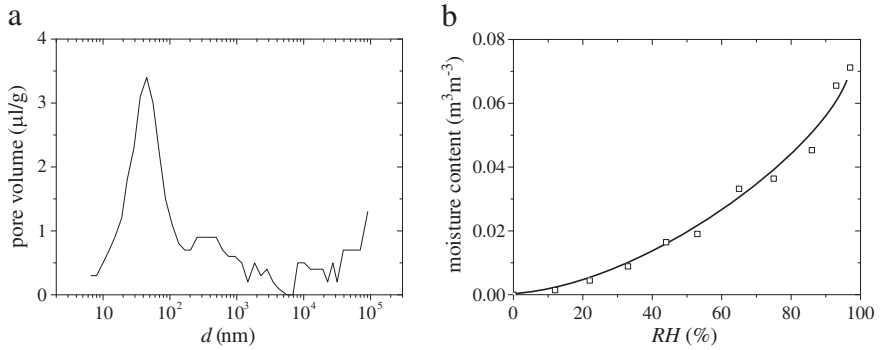

Fig. 2. a) The pore size distribution of the concrete measured by MIP. The pore sizes range from smaller than 10 nm to 100 μm. The dominant pore size is 30–40 nm. b) The sorption isotherm measured at 20 °C. The solid line is shown as a guide to the eye. Capillary saturation corresponds to a moisture content of 0.11 $m^3\ m^{-3}$.

was obtained by heating the sample up to a certain constant temperature above 100 °C. After the sample had reached a constant mass, the sample was slowly cooled down to room temperature under a 0% RH atmosphere. Thereby preventing any increase in moisture content or rehydration of the concrete. Then, at room temperature the NMR signal and mass were both measured. The results are shown in the inset of Fig. 3. A decrease in both signal and mass is observed for temperatures from 105 °C to 130 °C which can be attributed to adsorbed and chemically bound moisture. Note that in this temperature region the NMR signal dependence on mass is the same as for the free evaporable moisture content below 100 °C. For the drying temperatures of 130 °C to 250 °C the mass of the sample decreases indicating that chemically bound moisture is lost from the concrete. However, the NMR signal remains constant. For temperatures above 300 °C again both the signal and the moisture content decrease, until all signal is lost at a temperature between 500 and 800 °C.

From this drying experiment we can conclude that the NMR signal is linearly related to the free moisture content. Furthermore, the NMR setup is capable of measuring a signal from the chemically bound moisture content. Unlike in, e.g., gypsum there is no linear relation between the chemically bound moisture content and the NMR signal. In fact, between 130 and 250 °C no decrease in NMR signal is observed, although the mass of the sample decreases. Apparently, the moisture which is lost in this temperature range is not contributing to the overall NMR signal or it has a relaxation time which is too fast. At a temperature of 800 °C the concrete sample is completely dehydrated, resulting in zero NMR signal. In the future we will try to include the chemically bound moisture, but for now we will solely concentrate on the free moisture content.

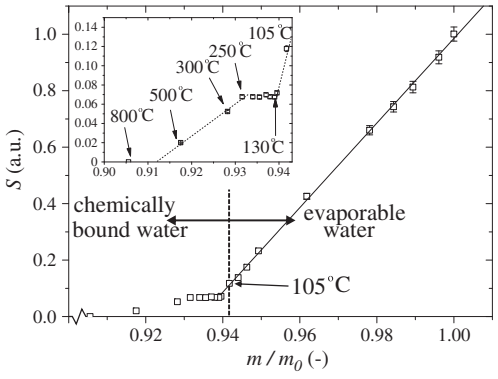

Fig. 3. The NMR signal calibration as a function of moisture content. The signal varies linearly with the amount of free moisture (solid line, $m/m_0>0.94$). The calibration of the non-evaporable moisture content (hydrated water) is shown in the inset. The temperatures indicate the temperature up to which the sample was heated. The background signal is 2×10^{-3}.

3. Results

In this section the moisture and temperature profiles are presented of four one-sided heating experiments on samples equilibrated at different relative humidities: 97, 86, 75, and 50% RH. We will start with the 97% RH experiment since in this experiment all the different moisture transport processes are captured. For the remaining three experiments we will suffice with only a short overview.

3.1. Concrete sample equilibrated at 97% RH

At the start of the experiment the concrete sample is in equilibrium with 97% RH, corresponding to a free moisture content of 0.07 $m^3\ m^{-3}$. The moisture and temperature profiles are shown in Fig. 4. The moisture profiles are normalised with respect to the first moisture profiles (bold line). As the surface (0 mm) is heated the temperature increases after 8.5 min to above 100 °C. The free moisture at the surface will boil and we can observe a boiling front developing at the surface. As the heating continues, the boiling front moves further into the material. To the left of the boiling front a zero free moisture content is measured. To provide a complete overview, we have chosen to include the signal originating from the chemically bound moisture. Therefore, the zero free moisture content level is indicated by $\theta=0$. However, it is possible for the signal to decrease below $\theta=0$, corresponding to loss of chemically bound moisture. As can be seen in Fig. 3 this is expected for temperature well above 250 °C.

The measured temperature profiles indicate that the boiling and dehydration processes have no significant influence on the heat transport. In previous heating experiments on fired-clay brick and calcium silicate brick a clear inflection in the temperature profiles was observed either caused by boiling and/or dehydration [17]. In this experiment, the moisture content of the concrete is relatively low and hence both the heat capacity, and thermal conductivity of the sample are dominated by the concrete heat capacity and conductivity.

As the boiling front moves further into the sample we can observe a significant increase in moisture content to the right of the boiling front. However, as the boiling front progresses the moisture content does not increase above approximately 0.11 $m^3\ m^{-3}$. This moisture content corresponds to the porosity of the concrete sample (indicated by the dashed line). The moisture content in this region cannot increase any further, because the material is saturated. To our knowledge this is the first direct and quantitative proof of so-called moisture clogging in concrete.

An explanation for the increase in moisture content can be found in the local vapour pressure at the boiling front. In Fig. 4b the

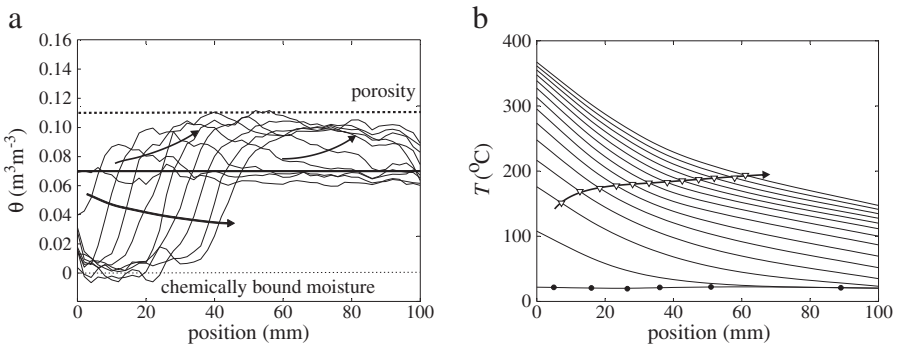

Fig. 4. Moisture and temperature profiles of a concrete sample heated from one side with 12 kW m^{-2}. At the start of the experiment the sample was equilibrated at 97% RH which corresponds to a moisture content of approximately 0.07 m^3 m^{-3}. The profiles are shown for every 8.5 min. The temperature at the boiling front is indicated by ▽ in the temperature profiles. The positions of the thermocouples are indicated by • in the first temperature profile. The evolution of the profiles in time is indicated by arrows.

temperature at the boiling front is indicated by ▽. The temperature at the front increases from approximately 160 °C to 195 °C. The saturated vapour pressures corresponding to these temperatures are 0.7 and 1.4 MPa, respectively, compared to 0.1 MPa atmospheric pressure. The increase above 100 °C (atmospheric boiling point) indicates that there is a local increased vapour pressure. The vapour pressure is assumed to be equal to the saturated vapour pressure. As a result of these high vapour pressures the vapour released at the boiling front is advected both towards the heated surface and the back of the sample. A temperature gradient is present across the sample. As a result the saturated vapour pressure immediately to the right of the boiling front is lower. The vapour advected to the back of the sample will therefore condensate, resulting in an increase of the free moisture content in the region to the right of the boiling front. The vapour advected towards the surface is able to exit the sample.

3.2. Equilibrated at 86, 75, and 50% RH

In this section we will give an overview of the results obtained from the samples in equilibrium with 86, 75, and 50% RH samples. The moisture and temperature profiles of these experiments are shown, from top to bottom, in Fig. 5. From the temperature profiles

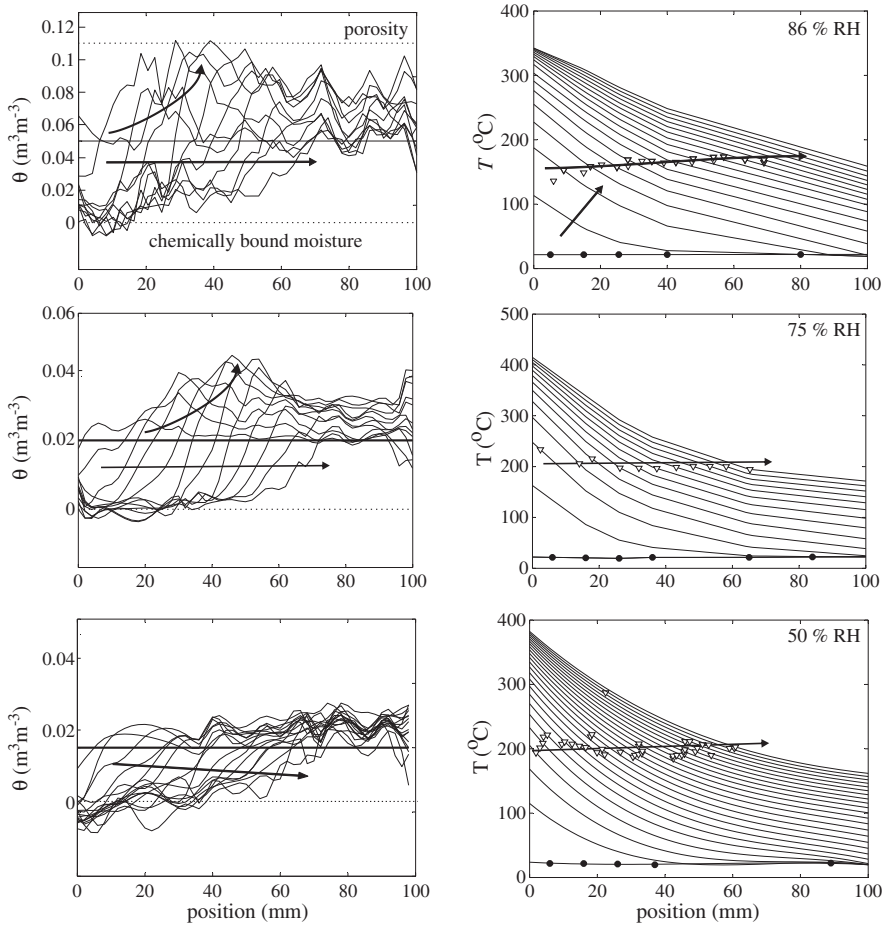

Fig. 5. Moisture and temperature profiles for three heating experiments: 86, 75, and 50% RH. The initial moisture contents of the samples are 0.05, 0.04, and 0.014 m^3 m^{-3}, respectively, and the profiles are shown for every 7, 8.5, and 6 min, respectively. The temperature at the boiling front is indicated by ▽ in the temperature profiles. The positions of the thermocouples are indicated by • in the first temperature profile.

it can be seen that both the heating rate and the maximum temperature of the three experiments are very similar to that of the 97% experiment.

We can identify a number of similar observations in all four experiments. At the start of the experiment a boiling front develops and moves through the sample. To the right of the boiling front in both the 86 and 75% RH samples a significant increase in moisture content is observed. In case of the 86% sample the maximum moisture content is close to saturation. In the 75% sample the maximum moisture content is still far from saturation. In the 50% experiment only a small increase in moisture content is observed. We can conclude that moisture clogging only occurs in both the 97 and the 86% samples, however in all cases condensation is observed. 97% sample does not show the same increase in moisture content strengthens the argument of the formation of a saturated region and the process of moisture clogging.

In the three experiments the temperatures at the boiling fronts are slightly higher than in the 97% sample, approximately 200 °C. The temperatures at the boiling front can be used to obtain the vapour pressures at the boiling front. The vapour pressures range from 1.5 to 1.9 MPa for the 75 and 50% sample to only 0.6 to 0.8 MPa for the 86% sample. An overview of the maximum vapour pressures at the boiling front is given in Table 2.

The positions of the moisture front and the 100 °C isotherms of all four experiments are shown in Fig. 6a. Although there is a large difference in moisture contents, all four samples show very similar results for both the speed of the 100 °C isotherm and boiling front. Although there are large differences in moisture content between the four samples, it does not significantly influence the movement of both the boiling and 100 °C front. We can conclude that the boiling and condensation processes do not influence the heat transport. Therefore in a simplified vapour transport model we can leave out the coupling between the heat and mass transfer.

3.3. Vapour transport model

We can introduce a relatively simple vapour transport model which can be used to describe the boiling front progression as a function of time. This model was introduced in a previous paper by van der Heijden et al. [17]. An overview of the model is shown in Fig. 7. Driven by the boiling process, a sharp boiling front will recede into the concrete, and its speed will be governed by the vapour flux from the drying front to the external surface. When the drying front advances a distance du in a time dt, a liquid water quantity per unit area of θdu is converted to vapour, where θ is the moisture content. This generates a vapour mass-flux J_v from the drying front to the external surface:

$$J_v = -\frac{\theta}{V_m}\frac{\partial u}{\partial t}, \tag{1}$$

with V_m the molar volume of liquid water. The vapour transport is assumed to be a viscous flow driven by the pressure gradient. Vapour is assumed to be the only gas phase present. Therefore, the vapour flux can be calculated from Darcy's law. We assume that the temperature gradient does not influence the vapour flux in the dry part, and that the vapour behaves as an ideal gas. The vapour flux J_v can now be expressed as a volume flux q times the density:

$$J_v = -\frac{k}{\mu}\frac{\partial p}{\partial x}\frac{p}{RT}, \tag{2}$$

where k is the vapour permeability, μ the viscosity of water, R the gas constant, T the temperature, and p is the pressure at the boiling front. In this model, the vapour flux is limited to one direction, i.e., towards the surface. This means that it can only be applied to saturated materials. Furthermore, there is no coupling between the mass and heat transfer, and the temperature increase in the material is completely determined by the concrete heat capacity. In the experiments presented in this paper the 86 and 97% samples are close to saturation.

If we equate Eq. 1 with Eq. 2, we obtain the following differential equation for the boiling front position:

$$\frac{\partial u}{\partial t} = \frac{kV_m}{2\mu RTn\theta}\frac{\Delta p^2}{u}, \tag{3}$$

The model has shown to accurately fit the boiling front movement in a variety of materials with the vapour permeability as the only free parameter [17].

We have used this model to fit the boiling front positions of the 97% experiment. In this experiment the material is saturated. Therefore, the assumption that the vapour is only advected towards the surface holds. The result is shown in Fig. 6b. The black dots indicate the measured front positions, and the solid line is the model fit with a relative permeability of $1\times10^{-16}\,m^2$. We have included the model results for two other permeabilities: 10^{-15} and $10^{-17}\,m^2$. It is clear that the speed of the boiling front is very sensitive to the vapour permeability. It must be noted that the vapour is transported through a concrete which is heated above 200 °C. Therefore, the obtained vapour permeability is not representative of the concrete at room temperature, it is the vapour permeability of a heated and degenerated porous material.

The four different concrete cores were drilled from the same batch of concrete. The samples were stored under the same conditions, until they were equilibrated with different relative humidities. Therefore, the vapour permeability should be in the same range. For the 86% RH sample we obtain a vapour permeability of $1\times10^{-16}\,m^2$, which is in agreement with the 97% sample, indicating that in fact the material is close to saturation. For the other two samples (50 and 75%), the obtained permeabilities are 2×10^{-17}, and 4×10^{-17}, respectively (see also Table 2). In these two experiments the samples are far from saturation, and the obtained values are significantly lower. By assuming the one directional vapour transport we make a maximum error of a factor of two. Furthermore, since concrete is a very heterogeneous material, it is not uncommon to observe a larger spread in permeability values obtained in several different samples, especially when the 'hot' vapour permeability is measured [21]. Therefore, the observed tendency may be fortuitous.

Table 2
Overview of the maximum vapour pressure and calculated vapour permeability of the four experiments.

RH (%)	p_v (MPa)	k_v (m^2)
50	1.5–1.9	2.10^{-17}
75	1.5–1.9	3.10^{-17}
86	0.6–0.8	1.10^{-16}
97	0.7–1.4	1.10^{-16}

4. Discussion and conclusions

We have shown that the NMR fire spalling setup is a very powerful tool in providing accurate moisture and temperature profiles. The moisture profiles can be measured with a resolution of 3–5 mm, while the sample is heated with a radiative heat flux of approximately 12 kW m^{-2}. The set of experiments with increasing moisture content which were presented reveals several important aspects of the moisture and heat transport. For the first time, the presented moisture profiles can be used to validate a number of moisture transport processes predicted since long by models.

First, the boiling and dehydration processes do not significantly influence the temperature distributions inside the sample. Immediately

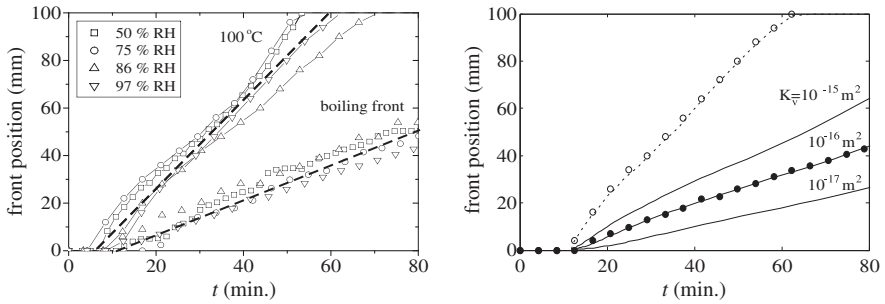

Fig. 6. a) Front positions of the 100 °C isotherm and the moisture fronts of the four different saturation experiments. b) The boiling front (•) and 100 °C isotherm positions (◦) of the 97% RH experiment are plotted as a function of time. The front positions are fitted using Eq. 1. The permeability which was used to fit the positions is 1×10^{-16} m^2. The results obtained for vapour permeability of 10^{-15} and 10^{-17} m^2 are included for comparison.

after the heating is started a boiling front is formed, indicating that the very low vapour permeability of the concrete prevents the moisture to redistribute in the time scale of the experiment.

Second, the temperatures measured at the boiling front are significantly higher than 100 °C, approximately 200 °C. This is a clear indication of an increased vapour pressure at the boiling front. In all four experiments a similar vapour pressure at the boiling front of approximately 1.4 MPa, yielded a tensile stress of 1.1 MPa [14]. If we assume a tensile strength of a concrete of 4 MPa, we can seen that in these experiments we are still far from any possible spalling related damage. However, the saturated vapour pressure increases significantly with temperature. The heating flux which was used in our experiments is still a factor of 10 lower than the heating flux in a large scale fire test or a real life fire. Increasing the heating flux tenfold, will most certainly result in vapour pressures at the boiling front comparable to or larger than the tensile strength.

To obtain the vapour pressures at the boiling front we have assumed a local thermal equilibrium. One can debate whether such an equilibrium exists inside the heated concrete. However, the heating rates in these experiments are limited to a maximum of approximately 15 °C min^{-1} and a thermal equilibrium is therefore expected. The calculated pressures are in the same order of magnitude as the vapour pressures measured in C30 concrete under a similar heating rates by Kalifa et al., namely ~ 1.6–1.8 MPa. Furthermore, they have shown that the vapour pressure as a function of temperature nicely obeys the saturated vapour pressure curve in case of a normal strength concrete [20]. More recently, Mindeguia et al. have measured the vapour pressures in the same experiment and found slightly lower vapour pressures ~0.2–0.6 MPa. It must be noted, that in their experiments the heating conditions were less severe [12].

Third, the first quantitative proof for the build up of a moisture peak is presented. While all moisture transport models predict the existence of such a peak, these predictions were never validated with moisture profile measurements. In the four experiments condensation results in an increase of moisture content. Moreover, the development of a saturated region has been shown in the 97% and 86% RH experiments. The saturated region will severely hinder the vapour transport to the back of the sample. However, we still observe an increase of moisture content at the back of the sample. It is possible that the vapour pressure to the left of the boiling front is high enough to push the liquid moisture further towards the back of the sample. In the introduction an example of water bleeding from the cold concrete surface was given. We have shown that a saturated region develops inside the concrete, and that the high vapour pressure might be able to push liquid water outside the sample. The region around the moisture peak is (partially) saturated, resulting in a very low capillary pressure.

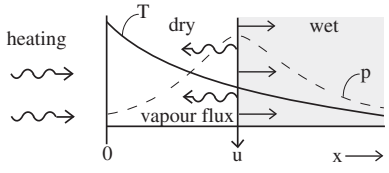

Fig. 7. Schematic overview of the model. The porous material is heated uniformly at its surface ($x=0$). Due to the heating the temperature T rises (solid line), and a receding drying front moves into the sample. This front is located at $x=u$ and separates the material into a dry and a wet part. The pressure (dotted line) will be highest at the drying front.

A simple vapour transport model was used to fit the boiling front positions as a function of time. The fit of the model resulted in a permeability of approximately 1×10^{-16} m^2 for the 97 and 86% RH samples. The model also describes the boiling front positions in the non-saturated samples with a similar vapour permeability. Already a very simple model with only one free parameter is capable in describing the main moisture transport features, i.e., the boiling front.

The combined moisture and temperature profiles are important for the validation of concrete fire spalling models. By combining the information already known from standard characterisation experiments with the NMR data, a full set of fire spalling parameters can be obtained for a certain concrete type. In this way, validated moisture and heat transfer models will be able to accurately predict the outcome of a fire inside a concrete structure.

Acknowledgements

This research was supported by the Dutch Technology Foundation, STW. The authors wish to thank Jef Noijen and Hans Dalderop for their help in the construction of the NMR setup and preparation of the temperature measurements.

References

[1] C.E. Majorana, V.A. Salomoni, G. Mazzucco, G.A. Khoury, An approach for modelling concrete spalling in finite strains, Mathematics and Computers in Simulation 80 (8) (2010) 1694–1712.
[2] P.C. Aitcin, Cements of yesterday and today — concrete of tomorrow, Cement and Concrete Research 30 (9) (2000) 1349–1359.
[3] G.N. Ahmed, J.P. Hurst, Modeling pore pressure, moisture, and temperature in high-strength concrete columns exposed to fire, Fire Technology 35 (3) (1999) 232–262.
[4] D. Gawin, F. Pesavento, B.A. Schrefler, Modelling of hygro-thermal behaviour of concrete at high temperature with thermo-chemical and mechanical material degradation, Computer Methods in Applied Mechanics and Engineering 192 (13–14) (2003) 1731–1771.
[5] X. Li, L. Rongtao, B.A. Schrefler, A coupled chemo-thermo-hygromechanical of concrete at high temperature and failure analysis, Internal journal for numerical and analytical methods in geomechanics 30 (2006) 635–681.
[6] B.A. Schrefler, G.A. Khoury, D. Gawin, C.E. Majorana, Thermo hydro-mechanical modelling of high performance concrete at high temperatures, Engineering Computations 19 (7) (2002) 787–819.
[7] M. Zeiml, R. Lackner, F. Pesavento, B.A. Schrefler, Thermo-hydrochemical couplings considered in safety assessment of shallow tunnels subjected to fire load, Fire safety journal 43 (2008) 83–95.

[8] J. Benard, R. Eymard, X. Nicolas, C. Chavant, Boiling in porous media: model and simulations, Transport in Porous Media 60 (1) (2005) 1–31.
[9] Abraham Dayan, Emil L. Gluekler, Heat and mass transfer within an intensely heated concrete slab, International Journal of Heat and Mass Transfer 25 (10) (1982) 1461–1467.
[10] C.L.D. Huang, Multiphase moisture transfer in porous-media subjected to temperature-gradient, International Journal of Heat and Mass Transfer 22 (9) (1979) 1295–1307.
[11] B.A. Schrefler, Multiphase flow in deforming porous material, International Journal for Numerical Methods in Engineering 60 (1) (2004) 27–50.
[12] J.C. Mindeguia, P. Pimienta, A. Noumowe, M. Kanema, Temperature, pore pressure and mass variation of concrete subjected to high temperature — experimental and numerical discussion on spalling risk, Cement and Concrete Research 40 (2009) 477–487.
[13] R. Jansson, L. Bostro¨m., Fire spalling — the moisture effect, 1st International workshop on concrete fire spalling due to fire exposure, 2009.
[14] Y. Ichikawa, G.L. England, Prediction of moisture migration and pore pressure build-up in concrete at high temperatures, Nuclear Engineering and Design 228 (1–3) (2004) 245–259.
[15] G.H.A. van der Heijden, H.P. Huinink, L. Pel, K. Kopinga, One dimensional scanning of moisture in heated porous building materials with NMR, Journal of Magnetic Resonance 208 (2) (2011) 235–242.
[16] G.H.A. van der Heijden, H.P. Huinink, L. Pel, K. Kopinga, Non isothermal drying of fired-clay brick, an NMR study, Chemical Engineering Science 64 (12) (2009) 3010–3018.
[17] G.H.A. van der Heijden, R.M.W. Bijnen, L. Pel, H.P. Huinink, Moisture transport in heated concrete, as studied by NMR, and its consequences for fire spalling, Cement and Concrete Research 37 (6) (2007) 894–901.
[18] K. Kopinga, L. Pel, One-dimensional scanning of moisture in porous materials with NMR, The Review of Scientific Instruments 65 (12) (1994) 3673–3681.
[19] D.R. Lide., Handbook of Chemistry and Physics, 90th edition CRC Press, 2009.
[20] P. Kalifa, F.D. Menneteau, D. Quenard, Spalling and pore pressure in HPC at high temperatures, Cement and Concrete Research 30 (12) (2000) 1915–1927.
[21] S. Dal Pont, B.A. Schrefler, A. Ehrlacher, Intrinsic permeability evolution in high temperature concrete: an experimental and numerical analysis, Transport in Porous Media 60 (2005) 43–74.

Notation

B_0: main magnetic field, T
B_1: radio — frequent magnetic field, T
G: gradient, Tm^{-1}
K: vapour permeability, m^2
V_m: molar volume water, $m^3\ mol^{-1}$
R: universal gas constant, $J\ K^{-1}\ mol^{-1}$
T: temperature, K
N: porosity, $m^3\ m^{-3}$
P: pressure, Pa

Greek symbols

Θ: moisture content, $m^3\ m^{-3}$
μ: viscosity, Pas
α: degree hydration
γ: gyromagnetic ratio, MHz/T